



UNIVERSITY OF LEEDS

This is a repository copy of *Familial autoinflammation with neutrophilic dermatosis reveals a regulatory mechanism of pyrin activation.*

White Rose Research Online URL for this paper:
<http://eprints.whiterose.ac.uk/98758/>

Version: Accepted Version

Article:

Masters, SL, Lagou, V, Jeru, I et al. (29 more authors) (2016) Familial autoinflammation with neutrophilic dermatosis reveals a regulatory mechanism of pyrin activation. *Science Translational Medicine*, 8 (322). RA45. ISSN 1946-6234

<https://doi.org/10.1126/scitranslmed.aaf1471>

Reuse

Unless indicated otherwise, fulltext items are protected by copyright with all rights reserved. The copyright exception in section 29 of the Copyright, Designs and Patents Act 1988 allows the making of a single copy solely for the purpose of non-commercial research or private study within the limits of fair dealing. The publisher or other rights-holder may allow further reproduction and re-use of this version - refer to the White Rose Research Online record for this item. Where records identify the publisher as the copyright holder, users can verify any specific terms of use on the publisher's website.

Takedown

If you consider content in White Rose Research Online to be in breach of UK law, please notify us by emailing eprints@whiterose.ac.uk including the URL of the record and the reason for the withdrawal request.



eprints@whiterose.ac.uk
<https://eprints.whiterose.ac.uk/>

Familial autoinflammation with neutrophilic dermatosis reveals a novel regulatory mechanism of pyrin activation

Seth L. Masters^{1,2*}, Vasiliki Lagou^{3,4,5*}, Isabelle Jéru^{6,7,8}, Paul J. Baker^{1,2}, Lien Van Eyck^{4,5}, David A. Parry⁹, Dylan Lawless¹⁰, Dominic De Nardo^{1,2}, Josselyn E. Garcia-Perez^{4,5}, Laura F. Dagley^{1,2,11}, Caroline Holley¹², James Dooley^{4,5}, Pierre-Yves Jeandel¹³, Raf Sciot^{14,15}, Dena Lyras¹⁶, Andrew I. Webb^{2,11}, Sandra E. Nicholson^{1,2}, Lien De Somer¹⁵, Erika van Nieuwenhove^{4,5,15}, Julia Ruuth-Praz^{7,8}, Bruno Copin⁸, Emmanuelle Cochet⁸, Myrna Medlej-Hashim¹⁷, Andre Megarbane^{18,19}, Kate Schroder¹², Sinisa Savic^{20,21}, An Goris³, Serge Amselem^{6,7,8}, Carine Wouters^{4,15*} and Adrian Liston^{4,5*}.

¹ Inflammation division, The Walter and Eliza Hall Institute of Medical Research, Parkville 3052, Australia

² Department of Medical Biology, The University of Melbourne, Parkville 3010, Australia

³ KUL - University of Leuven, Department of Neurosciences, Leuven, Belgium.

⁴ KUL - University of Leuven, Department of Microbiology and Immunology, Leuven,

Belgium.

⁵ Translational Immunology Laboratory, VIB, Leuven, Belgium

⁶ INSERM, UMR_S933, Paris, F-75012 France.

⁷ Université Pierre et Marie Curie-Paris, UMR_S933, Paris, F-75012 France.

⁸ Assistance Publique Hôpitaux de Paris, Hôpital Trousseau, Service de Génétique et

d'Embryologie médicales, Paris, F-75012 France.

⁹ Centre for Genomic & Experimental Medicine, Institute of Genetics & Molecular Medicine,

University of Edinburgh, Western General Hospital, Crewe Road South, Edinburgh, UK

¹⁰ Biomedical and Clinical Sciences, University of Leeds, Wellcome Trust Brenner Building,

St James's University Hospital, Leeds, UK

¹¹ Systems Biology and Personalised Medicine division, The Walter and Eliza Hall Institute of

Medical Research, Parkville 3052, Australia

¹² Cell Biology and Molecular Medicine division, Institute for Molecular Bioscience, The

University of Queensland, Brisbane, Queensland 4072, Australia

¹³ Département de Médecine Interne, Hôpital Archet 1, Université de Nice Sophia-Antipolis,

06202, Nice, France

¹⁴ KUL - University of Leuven, Department of Pathology, Leuven, Belgium.

¹⁵ University Hospitals Leuven, Leuven, Belgium.

¹⁶ Department of Microbiology, Monash University, Victoria 3800, Australia.

¹⁷ Department of Life and Earth Sciences, Faculty of Sciences II, Lebanese University,

Lebanon

¹⁸ Medical Genetics Unit, Faculty of Medicine, Saint Joseph University, Beirut, Lebanon

¹⁹ Institut Jérôme Lejeune, Paris, France

²⁰ Department of Clinical Immunology and Allergy, St James's University Hospital, Leeds,

UK

²¹ National Institute for Health Research–Leeds Musculoskeletal Biomedical Research Unit

(NIHR-LMBRU) and Leeds Institute of Rheumatic and Musculoskeletal Medicine (LIRMM),

Wellcome Trust Brenner Building, St James's University Hospital, Beckett Street, Leeds,

UK

*Equal authorship contribution.

Corresponding authors: Seth Masters, masters@wehi.edu.au, Carine Wouters,

carine.wouters@uzleuven.be, and Adrian Liston, adrian.liston@vib.be.

Abstract

Pyrin responds to pathogen signals and loss of cellular homeostasis by forming an inflammasome complex that drives the cleavage and secretion of IL-1 β . We studied a family with dominantly inherited autoinflammatory disease characterised by childhood-onset recurrent episodes of neutrophilic dermatosis, fever, elevated acute-phase reactants, arthralgia, and myalgia/myositis. Disease was caused by a mutation in *MEFV*, the gene encoding pyrin (S242R). The clinical distinction from FME, also caused by *MEFV* mutation, was due to loss of a 14-3-3 binding motif at phosphorylated S242. This interaction represents a guard regulating pyrin activation, which is downstream of bacterial effectors that trigger the pyrin inflammasome. S242R mutation recapitulated the effect of pathogen sensing, triggering inflammasome activation and IL-1 β production. Successful therapy targeting IL-1 β has been initiated in one patient, resolving Pyrin-Associated Autoinflammation with Neutrophilic Dermatitis (PAAND). This unique disease provides evidence that a guard mechanism, originally identified in plant innate immunity, also exists in humans.

Main text

Autoinflammatory diseases are characterized by recurrent episodes of fever with systemic and organ-specific inflammation, as well as uncontrolled activation of the innate immune response in the apparent absence of an infectious trigger(1). Familial Mediterranean fever (FMF, OMIM ID: 249100) is the most common of these monogenic diseases, characterized by short (24–72 h) episodes of fever associated with serositis, progressing to amyloidosis if untreated(2). FMF is an autosomal recessive disease caused by mutations in both alleles of the *MEFV* (*ME*diterranean *Fe*Ver) locus, which encodes the protein pyrin(3). Normally, pyrin functions as a link between intracellular pathogen sensing and activation of the inflammasome, allowing the production of inflammatory mediators during infection. As a potent checkpoint for the initiation of inflammation, the mechanisms of pyrin regulation are critical, and yet still poorly understood.

We studied a three-generation Belgian family of 22 individuals, of whom 12 developed autoinflammatory disease (**Figure 1a**). The disease was characterized by neutrophilic dermatosis, childhood-onset recurrent episodes of fever lasting several weeks, increased levels of acute-phase reactants, arthralgia and myalgia/myositis (**Figure 1b**). The neutrophilic dermatosis comprised a spectrum of clinical manifestations including severe acne, sterile skin abscesses, pyoderma gangrenosum and neutrophilic small vessel vasculitis (**Figure 1c,d**). Pathological examination of affected skin showed a dense, predominantly neutrophilic, vascular, perivascular and interstitial infiltrate (**Figure 1d**). Serum cytokine analysis revealed elevated inflammatory mediators such as IL-1 β , IL-6 and TNF α , and cytokines induced by inflammation such as IL-1Ra (**Figure 1e, Figure S1a**). One patient (III.3) presented with additional dilated cardiomyopathy at 13 years of age, which evolved into chronic cardiac decompensation necessitating cardiac transplantation at the age of 20 years. Analysis of a skeletal muscle biopsy from this patient indicated inflammatory infiltrate mainly comprised of

macrophages (**Figure S1b,c**). Due to the genetic causation by pyrin mutation (see below) and the characteristic features of systemic inflammation and dermatosis, we termed this disease Pyrin-Associated Autoinflammation with Neutrophilic Dermatitis (PAAND).

PAAND disease inheritance indicated a dominant mode of transmission (**Figure 1a**). We therefore performed genome-wide linkage analysis on 20 family members, revealing a genome-wide significant LOD score of 3.6 for a single region (1-6,283,321 on hg19) in chromosome 16 (**Figure S2**). Exome sequencing was performed on two linked trios within the pedigree (I.4, I.5 & II.6; II.8, II.9 & III.3), and we subjected the 8,720 variants within the linkage region to our filtering pipeline, identifying a single synonymous variant in *RPL3L*, and a single missense mutation in *MEFV* (rs104895127) (**Figure S3**). Inheritance of this mutation was directly tested in the remaining members of the pedigree, displaying complete segregation with disease (**Figure 1a**). The identified mutation was a C-to-G substitution at c.726 in exon 2 of *MEFV*, which results in a serine to arginine substitution at position 242 (S242R) in the pyrin protein. *MEFV* mutations are associated with the development of FMF, however the S242R mutation falls in a protein region distinct from that of typical FMF-associated mutations (**Figure S3**). A few cases of dominantly inherited FMF have been reported in the literature(4-6), however these are also not near S242R. While not falling within a characterized protein domain, Serine 242 is highly conserved across mammals (**Figure S3**) unlike some of the more typical FMF variants, that naturally occur in other species(7). Despite the association of *MEFV* mutations with FMF, the disease described here with S242R mutation is clinically distinct from FMF, with the absence of serositis and amyloidosis, the presence of severe recurrent neutrophilic dermatosis, and bouts of fever lasting several weeks rather than days (**Figure 1b**). Clinical cutaneous manifestations evoked a closer resemblance to pyogenic arthritis, pyoderma gangrenosum and acne (PAPA), which is caused by mutations

in the pyrin-binding partner *PSTPIP1*, although here too it was distinct, with a lack of pyogenic arthritis (**Figure 1b**).

To further investigate the physiological result of pyrin S242R mutation, we searched for other occurrences outside the investigated family. The variant was only seen in one out of 122,836 chromosomes in ExAC65000 (allele frequency= 8×10^{-6}), in a Colombian male for whom clinical information was not available (1000Genomes Phase 1 database), and was absent in 1087 unrelated Belgian exomes (available on NGS-Logistics(8)). Two other patients with the same mutation in *MEFV* had, however, been reported in the registry of mutations responsible for hereditary auto-inflammatory diseases (InFever, <http://fmf.igh.cnrs.fr/ISSAID/infevers/>) (9) and a third independent family was identified. The first was an individual from France with a heterozygous S242R mutation in the absence of any other coding *MEFV* mutations. Disease presentation was similar to the Belgian family, with recurrent inflammatory skin nodules associated with neutrophilic infiltrate and small vessel vasculitis, fever, arthralgia/myalgia and the absence of characteristic FMF symptoms, namely serositis and of amyloidosis (**Figure S4a**). The second individual was from Lebanon and carried the S242R mutation in conjunction with a known FMF variant M694V. New clinical analysis was not possible, however retrospective assessment of symptoms were somewhat characteristic for FMF, including periodic fevers of 3-5 days duration, joint pain and partial control of symptoms with colchicine treatment. Additional symptoms included recurrent aphthous ulcers, prompting an initial diagnosis of Behçets disease, chronically elevated CRP and transient skin rashes/nodules (**Figure S4b**). A third independent family was identified in the UK, and also demonstrated dominant inheritance of the PAAND phenotype (**Figure S4c**). Overall, the combination of inheritance in a pedigree exceptional by size, and confirmation of the mutation in three additional pedigrees with autoinflammatory features strongly supports the S242R mutation in pyrin as causative driver of PAAND.

The unique clinical presentation of the S242R mutations suggested a distinct regulatory mechanism of pyrin-mediated activation of the inflammasome. Therefore, we analysed ASC speck formation, which assembles as an intense cytoplasmic aggregate immediately downstream of pyrin(10). GFP-ASC was overexpressed in HEK293T cells at a level causing minimal spontaneous speck formation. Using this system the co-expression of pyrin led to increased spontaneous speck formation, which was further enhanced by the S242R mutation (**Figure 2a**). Quantification of ASC specks was performed by flow cytometry, using mCherry-tagged pyrin and further controlling for cells with similar expression levels of WT vs S242R pyrin (**Figure 2b**). The elevated speck formation of the S242R mutation was not observed from nearby heterozygous variants (R202Q and G304R) recently found in two Japanese patients who developed Sweet syndrome(11) (**Figure 2c**). Interestingly, typical FMF variants such as M680I and M694V did not lead to a significant increase in ASC specks in this assay, however when double mutant S242R/M694V pyrin was expressed, a significant increase was observed over the S242R single mutant protein (**Figure 2c**). Downstream of ASC, the S242R mutation resulted in Caspase-1 being activated, with increased production of the p20 subunit (**Figure 2d**) and incorporation into the inflammasome “speck” (**Figure S5**). To measure IL-1 β production, the human THP-1 monocytic cell line was used, with retroviral overexpression of WT or S242R pyrin. LPS was added for 24h to induce the synthesis of pro-IL-1 β , and a significant increase in mature, secreted IL-1 β was observed from cells expressing S242R pyrin compared to WT (**Figure 2e**). CRISPR-mediated deletion of endogenous human pyrin (*MEFV*^{-/-}) confirms that endogenous pyrin was not required for pyrin S242R activation, however deletion of endogenous Caspase-1 (*CASP1*^{-/-}) prevented IL-1 β production due to pyrin S242R (**Figure 2e**). Another known consequence of increased Caspase-1 activation is pyroptotic cell death, which was also increased by S242R expression (**Figure 2f**).

To more closely examine the molecular mechanism by which S242R regulates pyrin activity, we immunoprecipitated GST-tagged wildtype or S242R mutant protein from HEK293T cells. Eluates were run out on polyacrylamide gels and developed with a sensitive fluorescent protein stain, revealing a band that was specifically bound to the WT and not to the mutant protein (**Figure S6a**). Mass spectrometry analysis identified this band as containing the protein 14-3-3 (six out of seven human isoforms, **Figure S6b**). This interaction was then confirmed directly by western blot, using a pan-14-3-3 antibody (**Figure 3a**). Previously, two isoforms of 14-3-3 (epsilon [ε] and tau [τ]) were observed to interact with pyrin, dependent on phosphorylation of S242 and S208(12). In agreement with this, we could observe the phosphorylation of S242 in wildtype pyrin by mass spectrometry (**Figure S6c**). Recently, bacterial effectors that target RhoGTPases, such as TcdB, were reported to trigger pyrin activation(13). We therefore tested if their mechanism of action was similar to the S242R mutation, by releasing the inhibitory 14-3-3 protein, and this was indeed the case (**Figure 3b**). To confirm the phosphorylation status of S242, we employed an antibody that recognises the pSer 14-3-3 consensus motif (R/K x x pS x P; where x is any amino acid). Although S242 lacks the +2 proline, the antibody did detect a serine-phosphorylated form of pyrin, and this was destroyed by the S242R mutation (**Figure 3c**). Importantly, TcdB treatment also has the same effect, as the pSer 14-3-3 motif in pyrin can no longer be observed after TcdB exposure (**Figure 3c**). By contrast, the FMF mutations M680I, M694V and V726A had no appreciable effect on 14-3-3 binding or the pSer 14-3-3 motif in pyrin (**Figure S6d**). Therefore, FMF mutations are likely to affect pyrin activity via a separate mechanism, such as a structural rearrangement in the protein that facilitates inflammasome formation after pyrin activation, allowing FMF mutations to enhance disease presentation (**Figure S4b**) and ASC speck formation (**Figure 2c**). Together, these data reveal that nonphosphorylated S242, and removal

of 14-3-3 is the mechanism by which inhibition of RhoGTPases and the S242R mutation both activate the innate immune receptor pyrin.

These functional studies suggest that the S242R mutation drives disease in patients by removing the 14-3-3 guard from pyrin, allowing excessive IL-1 β production. In order to determine whether this process occurred in PAAND patients, we assessed mature IL-1 β production by patient monocytes. Monocytes from healthy individuals did not produce significantly increased levels of mature IL-1 β in response to LPS, a constraint partially imposed due to the guard-function of S242 phosphorylation, as high levels of mature IL-1 β were produced when TcdB was added in conjunction to LPS. By contrast, patient monocytes demonstrated a defect in guard-function, as LPS alone was sufficient to induce high levels of mature IL-1 β (**Figure 4a**). The dermal manifestations and relatively modest systemic upregulation of IL-1 β (Figure 1) suggested this process may be elevated in the tissues. In support of this, immunofluorescent analysis demonstrated elevated levels of cleaved (active) Caspase-1 and mature IL-1 β in skin biopsies from patients with PAAND (**Figure 4b**). Finally, the central role of this process in the pathogenesis of PAAND was tested through a clinical trial with anakinra (synthetic IL-1Ra). One of the patients from the UK (G1) was treated with anakinra, after she failed a course of corticosteroids and methotrexate. Shortly after starting anakinra (100 mg daily) her clinical symptoms resolved and, for the first time after several years during which her inflammatory markers were regularly measured, her CRP levels dropped to within normal limits (<5 mg/ml) (**Figure 4c**). These observations confirm that the consequences of constitutive pyrin inflammasome activation in PAAND are mediated by IL-1 β , and may be effectively controlled using IL-1 β antagonism.

The identification of a novel dominantly inherited autoinflammatory disease with severe neutrophilic dermatosis driven by pyrin S242R mutation greatly expands the spectrum of pyrin inflammasome-related disorders. Our analysis of the S242R mutation uncovered a novel

guard mechanism by which pyrin is regulated, with loss of S242 phosphorylation licensing pyrin for activation and IL-1 β maturation. The clinical features of PAAND, distinct from FMF, appear driven by local IL-1 β production, with antagonism of this pathway proving to be a successful therapy in one patient so far.

Given our results with TcdB, this study suggests that pyrin may sense pathogens through disruption of S242 phosphorylation. As yet, it is unknown as to whether TcdB and other pathogen signals inhibit the relevant kinase or activate a specific phosphatase, however the net effect is the release of the endogenous inhibitor of pyrin and the subsequent activation of the inflammasome. It is also conceivable that alterations in actin polymerisation that trigger pyrin activation(14) may also target S242 phosphorylation, or otherwise prevent 14-3-3 binding. Ancestrally, the phosphorylation and constitutive inhibition we observed for pyrin was first predicated in the guard hypothesis of plant innate immune defence by resistance proteins, some of which are regulated by Ser/Thr kinases(15). Phosphorylation may therefore more broadly negatively regulate other innate immune receptors such as NLRP3, where a mechanism of activation has to date proven elusive. In summary, our characterisation of a novel autoinflammatory disease, PAAND, identifies constitutive phosphorylation of S242 and the subsequent binding of 14-3-3 as a guard mechanism by which pyrin functions as an innate immune sensor.

Acknowledgements

We thank the patient families for participation in this study. We thank Dr Jae Jin Chae (NIH) and Prof Deborah Gumucio (University of Michigan) for providing pyrin, ASC and Caspase-1 expression constructs and Klara Mallants (KUL) for technical support. We thank Isabelle Touitou (Universite de Montpellier, INSERM U844), Nathalie Lucidarme, Klaas Vandevyvere, Paul Wynants, Petra De Haes and René Westhovens for patient care and clinical information. This work was supported by the ERC Start Grant IMMUNO (to A.L.), IUAP (T-

TIME), an F+ Postdoctoral Fellowship from the Research Fund KU Leuven (to V.L.), an FWO fellowship (L.V.E), grants from INSERM and GIS-Institut des Maladies Rares, Victorian State Government Operational Infrastructure Scheme Grant, and Project Grant (1057815), Program Grant (1016647), IRIISS Grant (361646) and fellowship (S.L.M.) from the Australian National Health and Medical Research Council (NHMRC).

Author contributions

SA and CW initiated the study. SLM, IJ, AG, SA, CW and AL designed and supervised the study. SLM, PJB, DD, LFD, CH, DL, AIW, SEN and KS are responsible for biochemical experiments to address the function of Pypin S242R. IJ, VL, LVE, DP, DL, JGP, JD, PYJ, RS, LDS, EN, JRP, BC, EC, MMH, AG, SS, SA, CA, CW and AL are responsible for genetic and pathologic examination of patients. SLM, CW and AL wrote the paper with contributions from all authors.

References

1. S. Federici *et al.*, Evidence-based provisional clinical classification criteria for autoinflammatory periodic fevers. *Annals of the rheumatic diseases* **74**, 799-805 (2015).
2. F. M. F. C. French, A candidate gene for familial Mediterranean fever. *Nature genetics* **17**, 25-31 (1997).
3. S. L. Masters, A. Simon, I. Aksentijevich, D. L. Kastner, Horror autoinflammaticus: the molecular pathophysiology of autoinflammatory disease (*). *Annual review of immunology* **27**, 621-668 (2009).
4. A. Aldea *et al.*, A severe autosomal-dominant periodic inflammatory disorder with renal AA amyloidosis and colchicine resistance associated to the MEFV H478Y variant in a Spanish kindred: an unusual familial Mediterranean fever phenotype or another MEFV-associated periodic inflammatory disorder? *Am J Med Genet A* **124A**, 67-73 (2004).
5. D. R. Booth *et al.*, The genetic basis of autosomal dominant familial Mediterranean fever. *QJM* **93**, 217-221 (2000).
6. M. Stoffels *et al.*, MEFV mutations affecting pyrin amino acid 577 cause autosomal dominant autoinflammatory disease. *Annals of the rheumatic diseases* **73**, 455-461 (2014).
7. P. Schaner *et al.*, Episodic evolution of pyrin in primates: human mutations recapitulate ancestral amino acid states. *Nature genetics* **27**, 318-321 (2001).
8. A. Ardeshirdavani *et al.*, NGS-Logistics: federated analysis of NGS sequence variants across multiple locations. *Genome medicine* **6**, 71 (2014).
9. I. Touitou *et al.*, Infervers: an evolving mutation database for auto-inflammatory syndromes. *Hum Mutat* **24**, 194-198 (2004).

10. A. L. Waite *et al.*, Pypin and ASC co-localize to cellular sites that are rich in polymerizing actin. *Exp Biol Med (Maywood)* **234**, 40-52 (2009).
11. T. Jo, K. Horio, K. Migita, Sweet's syndrome in patients with MDS and MEFV mutations. *The New England journal of medicine* **372**, 686-688 (2015).
12. I. Jeru *et al.*, Interaction of pypin with 14.3.3 in an isoform-specific and phosphorylation-dependent manner regulates its translocation to the nucleus. *Arthritis Rheum* **52**, 1848-1857 (2005).
13. H. Xu *et al.*, Innate immune sensing of bacterial modifications of Rho GTPases by the Pypin inflammasome. *Nature* **513**, 237-241 (2014).
14. M. L. Kim *et al.*, Aberrant actin depolymerization triggers the pypin inflammasome and autoinflammatory disease that is dependent on IL-18, not IL-1beta. *J Exp Med* **212**, 927-938 (2015).
15. J. L. Dangl, J. D. Jones, Plant pathogens and integrated defence responses to infection. *Nature* **411**, 826-833 (2001).

Figure 1. Clinical and immunological features of Pyrin Associated Autoinflammation with Neutrophilic Dermatitis (PAAND). (a) Dominant inheritance of PAAND over three generations, with complete penetrance observed for the S242R mutation (*MEFV* c.C726G, denoted CG). Trios indicated by red boxing were subjected to exome sequencing. (b) 22 family members were assessed for neutrophilic dermatosis, recurrent childhood-onset fever, acute-phase reactants, arthralgia, myalgia, cardiomyopathy, anemia, pyogenic arthritis and serositis across three generations (G1, G2, G3). ND, not determined; *, recent onset. (c) Typical macroscopic features (pyoderma lesions on the arm, top, and pustular acne lesions on the face, bottom) (representative from patient II.7). (d) Histologic presentation of inflammatory infiltrate in the subcutis, involving subcutaneous vessels and extending into the surrounding panniculus and deep dermis. Scale bar = 500um. Higher magnification shows predominantly polymorphonuclear vascular and perivascular infiltrate (representative from patient II.7). Scale bar = 50um. (e) Serum levels of IL-1 β , IL-1Ra and IL-6 in patients during inflammatory episodes (n=6) and healthy controls (n=121). For healthy controls box and whiskers represent 25-75% and 5-95% range. For patients, mean and standard deviation shown. ***, p<0.001; ****, p<0.0001.

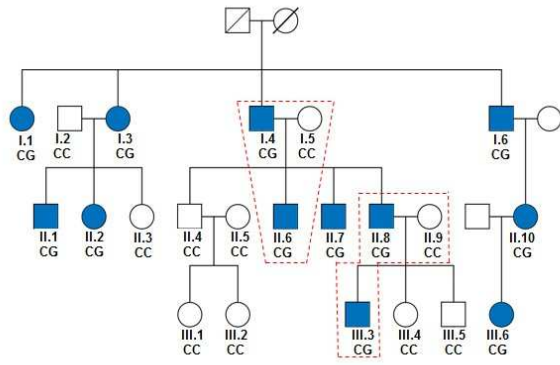
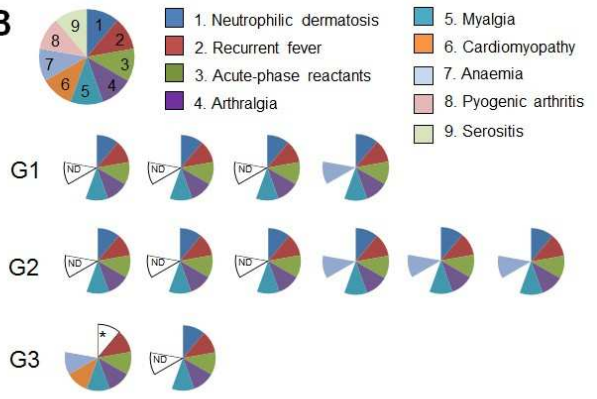
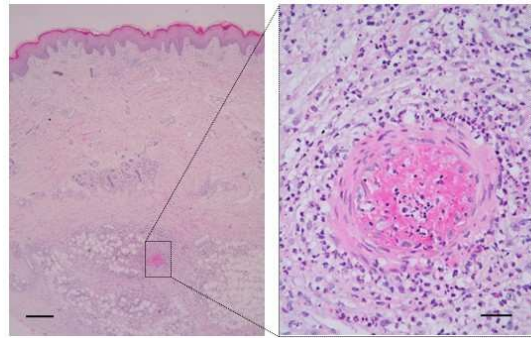
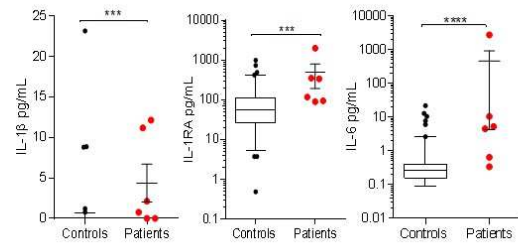
A**B****C****D****E**

Figure 2. Spontaneous inflammasome activation by pyrin S242R. **(a)** Confocal microscopy showing a pyrin-driven increase in cytoplasmic specks of GFP-tagged ASC when co-transfected into HEK293T cells with wildtype or mutated pyrin (S242R). **(b)** Representative FACS analysis of GFP-ASC specks with pyrin and pyrin S242R. **(c)** Quantification of 3 biological replicates for GFP-ASC specks by flow cytometry, with different pyrin mutants. **(d)** Western blots for active Caspase-1 (p20 subunit) following expression of Caspase-1 and ASC in HEK293T cells, together with an increasing concentration of Myc-tagged pyrin or pyrin (S242R). **(e)** Monocytic THP-1 cells where Caspase-1 or pyrin were deleted by CRISPR, then reconstituted by retroviral expression of pyrin or pyrin (S242R). IL-1 β was measured by ELISA, and **(f)** cell death quantified by PI staining and flow cytometry 24hrs after stimulation with LPS. All experiments repeated at least 3 times. All representative of at least 3 biologically-independent experiments. Error bars represent mean + SD for 3 biological replicates, *****, $p < 0.0001$.

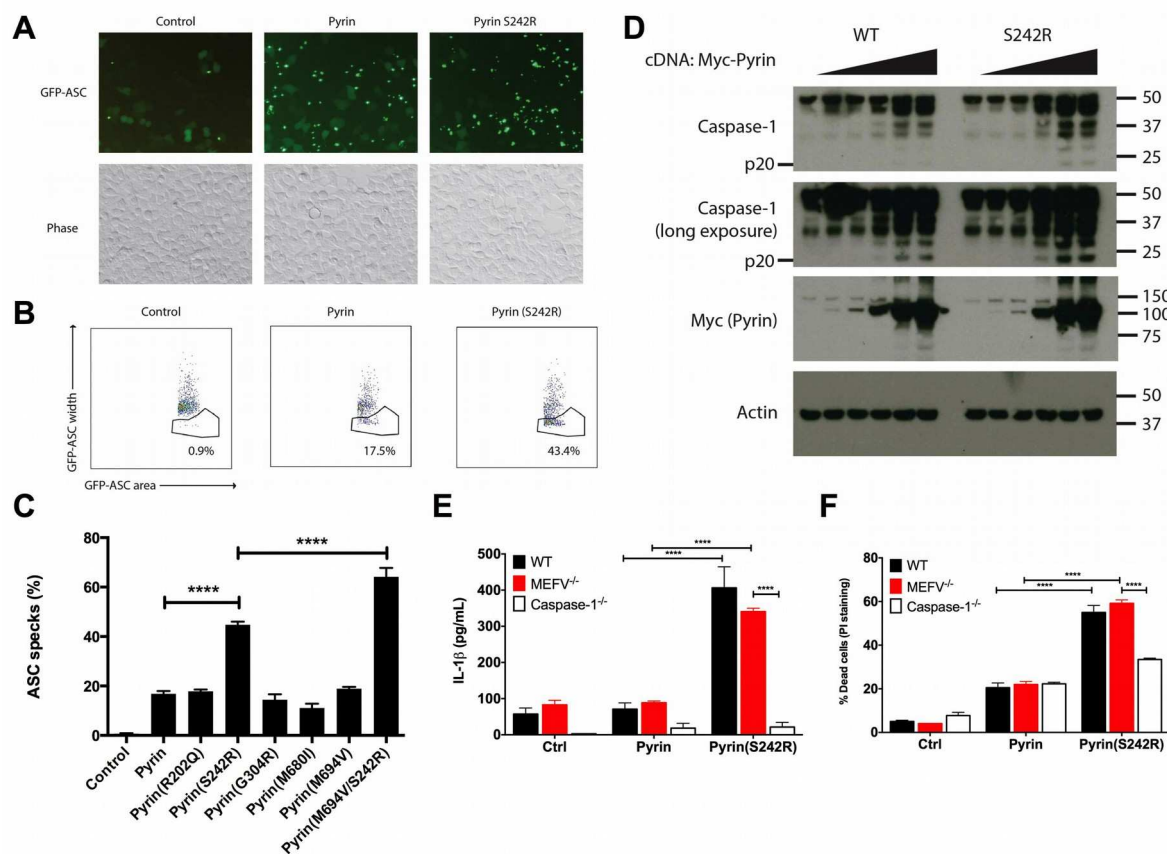


Figure 3. Guard mechanism of pyrin activation. (a) Pyrin with or without the S242R variant was overexpressed in HEK293T cells and immunoprecipitated by virtue of a GST-tag. Eluates were examined by western blotting, probing for endogenous (pan)14-3-3, with GST (pyrin) and (pan)14-3-3 also quantified in the starting lysates. (b) HEK293T cells expressing GST alone or GST-pyrin were treated with or without TcdB for 6 h prior to lysis and analysed as in (a). (c) HEK293T cells expressing GST-tagged pyrin or S242R pyrin were left untreated or treated with TcdB as in (b), then immunoprecipitated prior to western blotting for pSer(14-3-3 motif) and GST (pyrin). All representative of at least 3 biologically-independent experiments.

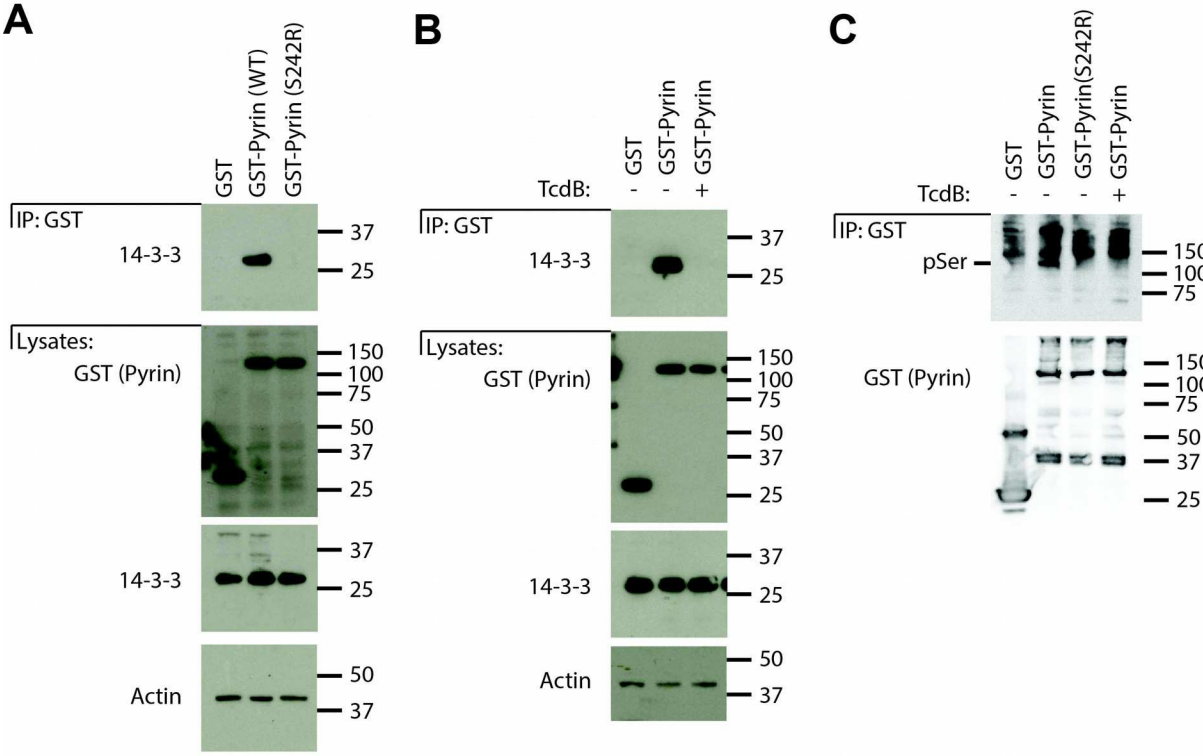
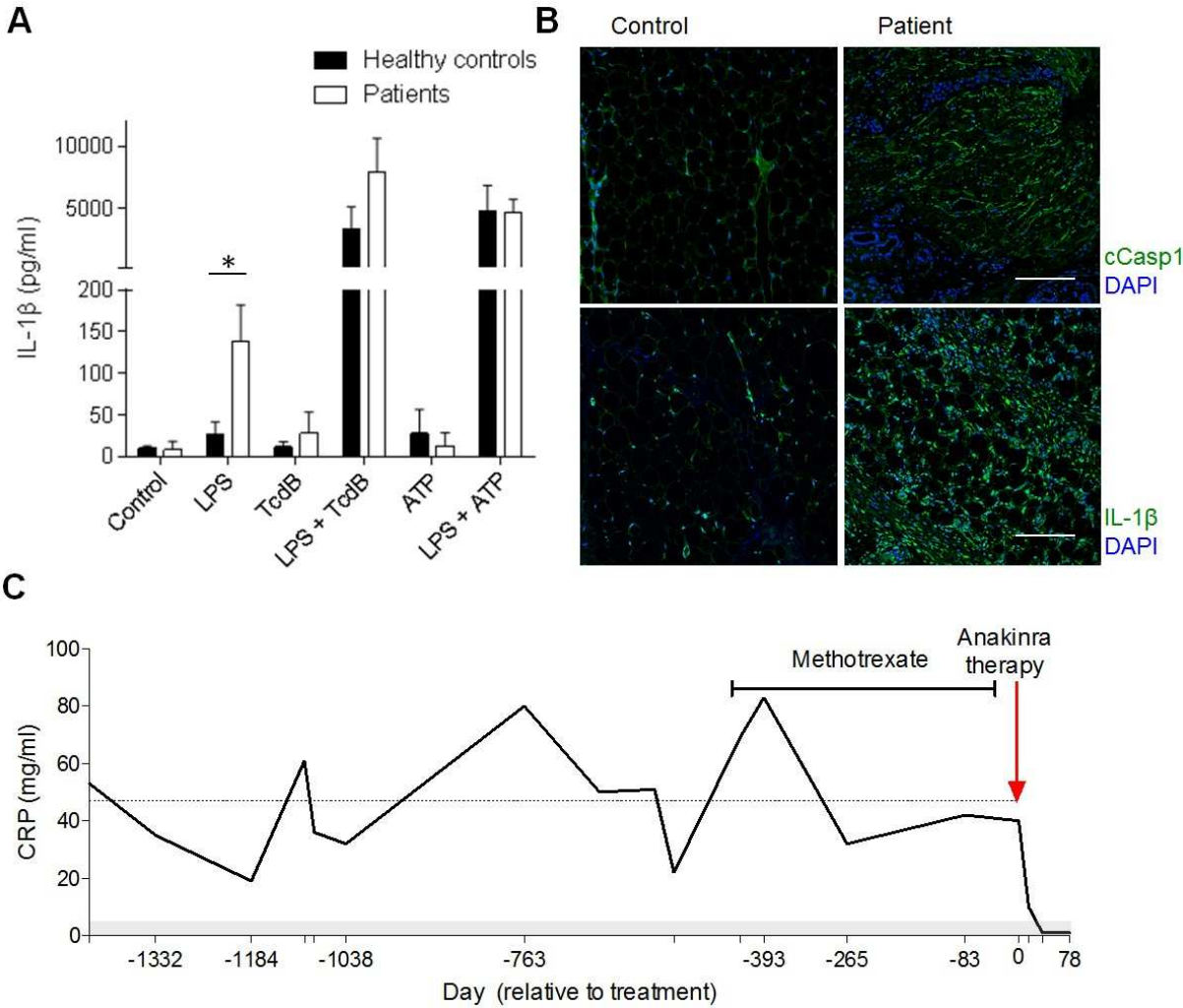


Figure 4. PAAND is driven by local inflammasome activation and IL-1 β production. (a)

Monocytes were purified from three PAAND patients and three healthy controls prior to stimulation for one hour with LPS \pm ATP, or \pm TcdB. Mature IL-1 β was measured in the supernatant. Means + SD for n=3 *, p<0.05. **(b)** Immunofluorescence staining for cleaved Caspase-1 and mature IL-1 β in healthy control skin and an affected biopsy from patient III.3 (bar = 200 μ m). **(c)** CRP levels were measured before and after treatment with 100mg/day Anakinra (day 0) in UK patient G1. Dashed line indicates three-year average CRP level prior to treatment, arrow indicates initiation of treatment, ticks indicate sample points, gray zone indicates normal CRP range.



Familial autoinflammation with neutrophilic dermatosis reveals a novel regulatory mechanism of pyrin activation

Seth L. Masters^{1,2*}, Vasiliki Lagou^{3,4,5*}, Isabelle Jéru^{6,7,8}, Paul J. Baker^{1,2}, Lien Van Eyck^{4,5}, David A. Parry⁹, Dylan Lawless¹⁰, Dominic De Nardo^{1,2}, Josselyn E. Garcia-Perez^{4,5}, Laura F. Dagley^{1,2,11}, Caroline Holley¹², James Dooley^{4,5}, Pierre-Yves Jeandel¹³, Raf Sciot^{14,15}, Dena Lyras¹⁶, Andrew I. Webb^{2,11}, Sandra E. Nicholson^{1,2}, Lien De Somer¹⁵, Erika van Nieuwenhove^{4,5,15}, Julia Ruuth-Praz^{7,8}, Bruno Copin⁸, Emmanuelle Cochet⁸, Myrna Medlej-Hashim¹⁷, Andre Megarbane^{18,19}, Kate Schroder¹², Sinisa Savic^{20,21}, An Goris³, Serge Amselem^{6,7,8}, Carine Wouters^{4,15*} and Adrian Liston^{4,5*}.

¹ Inflammation division, The Walter and Eliza Hall Institute of Medical Research, Parkville 3052, Australia

² Department of Medical Biology, The University of Melbourne, Parkville 3010, Australia

³ KUL - University of Leuven, Department of Neurosciences, Leuven, Belgium.

⁴ KUL - University of Leuven, Department of Microbiology and Immunology, Leuven, Belgium.

⁵ Translational Immunology Laboratory, VIB, Leuven, Belgium

⁶ INSERM, UMR_S933, Paris, F-75012 France.

⁷ Université Pierre et Marie Curie-Paris, UMR_S933, Paris, F-75012 France.

⁸ Assistance Publique Hôpitaux de Paris, Hôpital Trousseau, Service de Génétique et d'Embryologie médicales, Paris, F-75012 France.

⁹ Centre for Genomic & Experimental Medicine, Institute of Genetics & Molecular Medicine,

University of Edinburgh, Western General Hospital, Crewe Road South, Edinburgh, UK

¹⁰ Biomedical and Clinical Sciences, University of Leeds, Wellcome Trust Brenner Building,

St James's University Hospital, Leeds, UK

¹¹ Systems Biology and Personalised Medicine division, The Walter and Eliza Hall Institute of Medical Research, Parkville 3052, Australia

¹² Cell Biology and Molecular Medicine division, Institute for Molecular Bioscience, The

University of Queensland, Brisbane, Queensland 4072, Australia

¹³ Département de Médecine Interne, Hôpital Archet 1, Université de Nice Sophia-Antipolis, 06202, Nice, France

¹⁴ KUL - University of Leuven, Department of Pathology, Leuven, Belgium.

¹⁵ University Hospitals Leuven, Leuven, Belgium.

¹⁶ Department of Microbiology, Monash University, Victoria 3800, Australia.

¹⁷ Department of Life and Earth Sciences, Faculty of Sciences II, Lebanese University,

Lebanon

¹⁸ Medical Genetics Unit, Faculty of Medicine, Saint Joseph University, Beirut, Lebanon

¹⁹ Institut Jérôme Lejeune, Paris, France

²⁰ Department of Clinical Immunology and Allergy, St James's University Hospital, Leeds,

UK

²¹ National Institute for Health Research–Leeds Musculoskeletal Biomedical Research Unit

(NIHR-LMBRU) and Leeds Institute of Rheumatic and Musculoskeletal Medicine (LIRMM),

Wellcome Trust Brenner Building, St James's University Hospital, Beckett Street, Leeds,

UK

*Equal authorship contribution.

Corresponding authors: Seth Masters, masters@wehi.edu.au, Carine Wouters,

carine.wouters@uzleuven.be, and Adrian Liston, adrian.liston@vib.be.

Table of contents

4..... Methods

9..... Figure S1

10..... Figure S2

11..... Figure S3

12..... Figure S4

13..... Figure S5

14..... Figure S6

15..... References

Methods

Human subjects

We documented 22 family members from three generations, all of Flemish (Belgian) ancestry. The family included 12 patients (seven males and five females) with a clinical combination of childhood onset episodes of myalgia/myositis and neutrophilic dermatosis (pyoderma gangrenosum, acne, cutaneous small vessel vasculitis), increasing in severity with age. The remaining 10 family members were healthy with no apparent symptoms. Additional pedigrees were included from the UK, France and Lebanon. Written informed consent was obtained from each participant, and the study was approved by the ethical committee of UZ Leuven (S52653), the Espace Ethique/Université Saint Joseph - Liban and the Comité de Protection des Personnes Ile-de-France 5 (Paris, France). Patients from the UK were consented under ethical approval for molecular genetics research studies obtained from South Yorkshire Research Ethics Committee (REC ref. no. 11/H1310/1). Written informed consent to publish images of patients' symptoms was obtained.

Genetic linkage and whole-exome sequence analysis

Whole-genome genotyping for 20 family members (affected and healthy) was performed using the Infinium Human Linkage-12 Genotyping BeadChip (Illumina, San Diego, CA). The BeadChip includes 6,090 common single-nucleotide polymorphism markers with an average spacing of 441kb and 0.58cM across the genome. Linkage analysis was performed with the Merlin 1.1.2 software assuming autosomal dominant inheritance, full penetrance, no consanguinity and a mutation allele frequency of 0.0001. Candidate genes were ranked according to expression in human peripheral blood leukocytes¹.

Whole-exome sequencing was performed for two trios, i.e. the proband and both parents. This corresponds to three affected (Family Members III-3, I-4, II-6, II-8) and two healthy family

members (I-5 and II-9). Genomic DNA samples for whole-exome sequencing were prepared from heparinized peripheral blood using the FlexiGene kit (QIAGEN, Hilden, Germany). Exome sequence libraries were prepared using a SeqCap EZ Human Exome Library v3.0 kit (Roche NimbleGen, Madison, Wisconsin, USA). Paired-end sequencing was performed on the Illumina HiSeq2000 (Genomics Core Facility, University of Leuven, Belgium). Alignment of the sequence reads to the Human Reference Genome Build hg19, variant calling and annotation was done with a pipeline based on BWA², GATK HaploTypeCaller^{3,4} and Annovar⁵. The samples sequenced had an average of 98.2 (range 57.7-127.8) million reads with 93% [range 87.2-94.3] to 81% [range 57.1-88.8] of targeted bases being covered at ≥ 10 -fold or 30-fold, respectively. In order to select candidate genes the following variants were considered: i) compatible with the presumed mode of inheritance, i.e. heterozygous in affected individuals and not present in healthy ones, ii) overlapping a coding exon or within 2bp of a splicing junction, iii) not synonymous, iv) not present in genomic duplications, v) allele frequency ≤ 0.01 in 65000 Exome Aggregation Consortium (ExAC65000), vi) absent in 1087 unrelated Belgian individuals without the disease. The pyrin variant identified, rs104895178, has merged into rs104895127. The variation was validated by Sanger sequencing of exon 2 on an ABI 3730 XL Genetic Analyzer (Applied Biosystems). Sequencing data was analysed using the Staden package software.

Cytokine analysis

Plasma samples collected from patients and controls were stored at -80°C . Cytokine levels in plasma were quantified by an electrochemiluminescence immunoassay format using Meso Scale Discovery (MSD) plates according to manufacturer's instructions. Data was analyzed with Discovery Workbench® 4.0. Plasma IL-1Ra levels were measured using a human IL-1Ra ELISA (Thermo Fisher Scientific) according to manufacturer's instructions.

Monocytes were isolated from peripheral blood mononuclear cells of patients and controls using CD14 Microbeads (Miltenyi Biotec) and cultured overnight. The next day the cells were primed with 200 ng/mL UltraPure LPS (Invivogen) for 1 hour before addition of 1 µg/ml TcdB (Abcam) or 5 mM ATP (Invivogen). Supernatants were collected after 1 hour and IL-1 levels were measured by ELISA (R&D Systems).

Cell culture

HEK293T cells were transfected using Lipofectamine (Life Technologies) according to manufacturer's instructions, using constructs for human Myc-, mCherry- or GST-pyrin⁶, Myc- or GFP-ASC⁷, Myc- or GFP-Caspase-1⁸ or HA-14-3-3β (Addgene). *MEFV* mutations were created by site-directed mutagenesis using the QuikChange Lightning Multi Site-Directed Mutagenesis Kit (Agilent). The *CASP1* KO THP-1 cells, techniques for lentivirus production and CRISPR/Cas9-based knockout have been previously described⁹. *MEFV*-specific sgRNAs (exon 1 GGCGTACTCTTCCCCATAGT, exon 2 TCTAGGTCGCATCTTTCCCG) were ligated into the *BsmBI* restriction site on the doxycycline-inducible sgRNA vector. Complementation was performed using retrovirus expressing *MEFV* cDNA from a pLNCX2 backbone⁶. To activate pyrin and induce IL-1ε production and pyroptosis *in vitro*, THP-1 cells were primed with 200 ng/mL UltraPure *E. coli* EH100 (Ra) LPS (Enzo Life Sciences) for 30 minutes before addition of 200 nM TcdB. Cells were incubated for 20 hours before measuring IL-1β release by ELISA (R&D Systems) and cell death by propidium iodide (Sigma-Aldrich) staining at 1 βg/mL and flow cytometry. All cell lines originally from ATCC, and tested for mycoplasma contamination.

Western blotting and immunoprecipitation

For western blotting, THP-1 monocytes were lysed in RIPA buffer, for immunoprecipitation HEK293T cells were lysed in NP-40 lysis buffer supplemented with protease inhibitor

(complete protease inhibitor cocktail, Roche). Immunoprecipitation was performed using glutathione sepharose 4B (GE healthcare), with samples eluted in SDS-reducing sample buffer. Eluates were run on SDS polyacrylamide gels and treated as below for mass spectrometry, or routine western blotting was performed using the following antibodies: Pypin (AdipoGen rabbit μ -pypin, AL196), Caspase-1 (Adipogen mouse α -Caspase-1 p20, Casper-1), GST (mouse α -GST, in-house), HA (Covance mouse α -HA1.1), 14-3-3 (Santa Cruz goat mouse α -14-3-3, sc-629), actin (Santa Cruz goat α -actin, sc-1616) and pSer (Cell signaling mouse α -pSer 14-3-3 binding motif, #9601).

Mass spectrometry analysis

Samples were run on SDS polyacrylamide gels, stained using Sypro Ruby (Bio-Rad) and subsequently Coomassie G-250. Bands of interest were excised and subjected to reduction, alkylation and LysargiNase¹⁰ digestion prior to mass spectrometry analysis essentially as previously described¹¹. Raw files consisting of high-resolution MS/MS spectra were processed with MaxQuant (version 1.5.2.8). Extracted peak lists were searched against the human protein sequences obtained from the Uniprot, Swissprot and Ensembl knowledge bases. Cleavage specificity was set using [X|K/R] as a simple cleavage site rule for LysargiNase allowing up to 3 missed cleavages.

Fluorescence microscopy and cytometry

GFP-ASC specks were imaged in HEK293T cells using an Olympus IX70 inverted microscope with 20x objective. Specks were also quantified by flow cytometry¹². In brief, cells gated based on viability and moderate mCherry (pypin) expression were then selected for calculation of the percentage of cells containing an ASC speck, defined by GFP-width vs GFP-area profiles. Immunofluorescence was performed on skin sections fixed in 10% neutral

formalin, embedded in paraffin and antigen retrieved with pH 9.0 Tris. Sections were blocked, stained with rabbit anti-IL-1 (ab2105, Abcam) and cleaved Caspase-1 (4199, Cell Signalling), prior to developing with donkey anti-rabbit 488 (A-21206, Life Technologies) and DAPI (D1306, Life Technologies). Sections were mounted and cover-slipped using fluoromount G (Southern Biotech) before images were acquired with an LSM 510 Meta confocal microscope (Zeiss).

Figure S1. Inflammatory manifestations of PAAND. (a) Serum levels of IL-2, IFN γ , IL-4, IL-17, IL-10, IL-12, IL-13 and TNF α in patients during inflammatory episodes (n=6) and healthy controls (n=121). For healthy controls box and whiskers represent 25-50% and 5-95% range. For patients, mean and standard deviation shown. ***, p<0.001; ****, p<0.0001. **(b)** Histologic presentation of inflammatory infiltrate in the skeletal muscle of patient III.3. Mononuclear infiltrate in the perimysium by H&E (bar = 50 μ m) is shown at higher magnification. **(c)** Macrophages were assessed through CD68 immunohistochemistry in the skeletal muscle of patient III.3 (bar = 50 μ m).

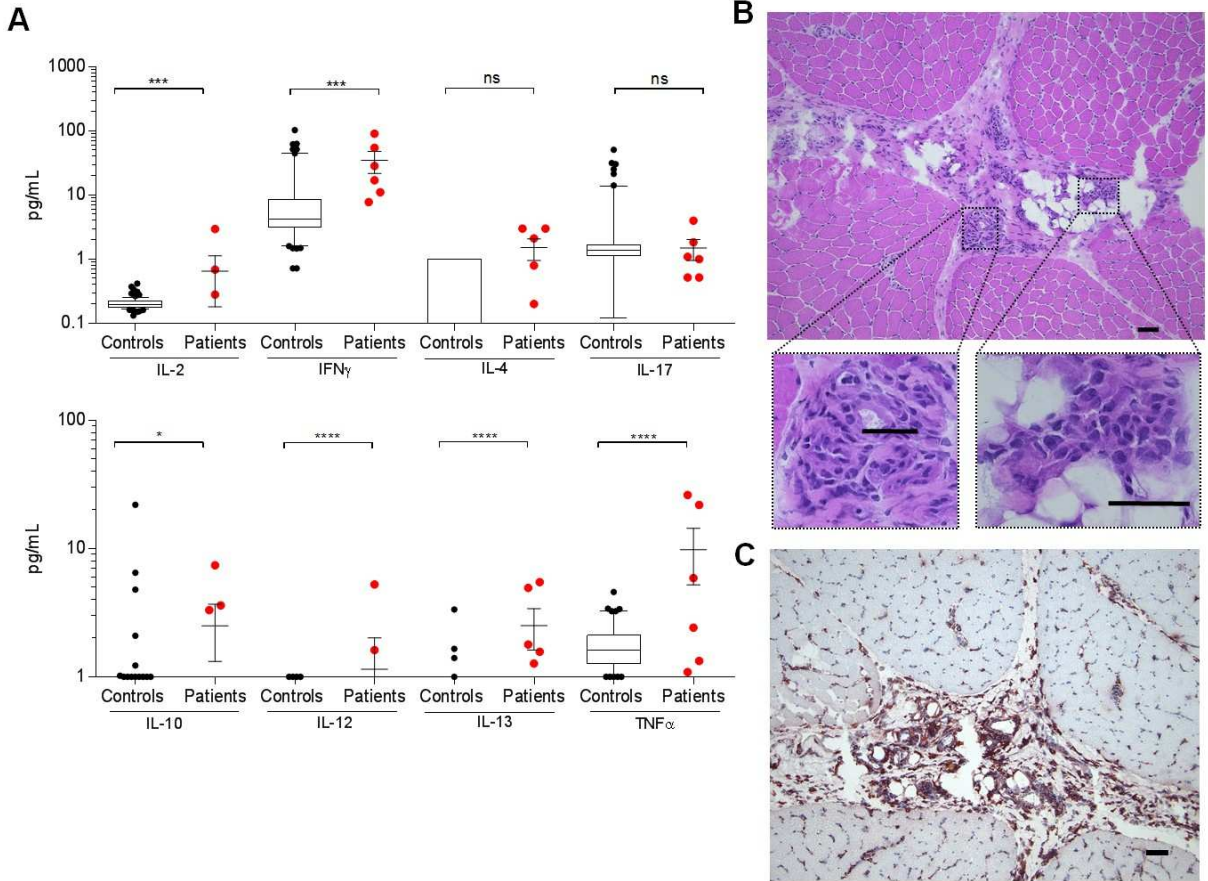


Figure S2. Results from linkage analysis. Genome-wide analysis for 20 family members (12 affected, 10 unaffected), indicating LOD scores for each chromosome.

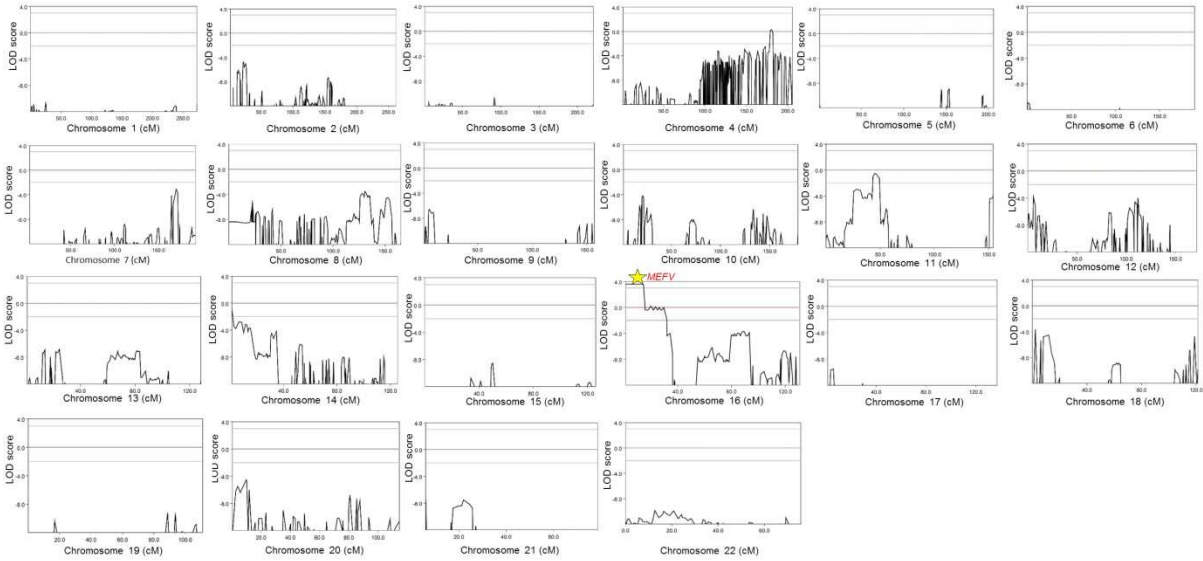


Figure S3. Dominant inheritance of PAAND caused by mutation in pyrin, S242R. (a) The gene-structure of the linkage (Chr16:1-6,283,321), indicating average fold coverage in patients and genes with differential expression in peripheral blood leukocytes. Exome sequencing in this region identified a single synonymous variant in *RPL3L*, and a single missense mutation in *MEFV*. **(b)** Domain structure of pyrin, indicating the locations of the observed S242R mutation (yellow star), known autosomal dominant mutations causing FMF (orange) and known autosomal recessive mutations causing FMF (blue). **(c)** Cross-species conservation of pyrin in the region flanking S242. The background colour indicates the level of conservation (red for highly conserved positions and blue for less conserved).

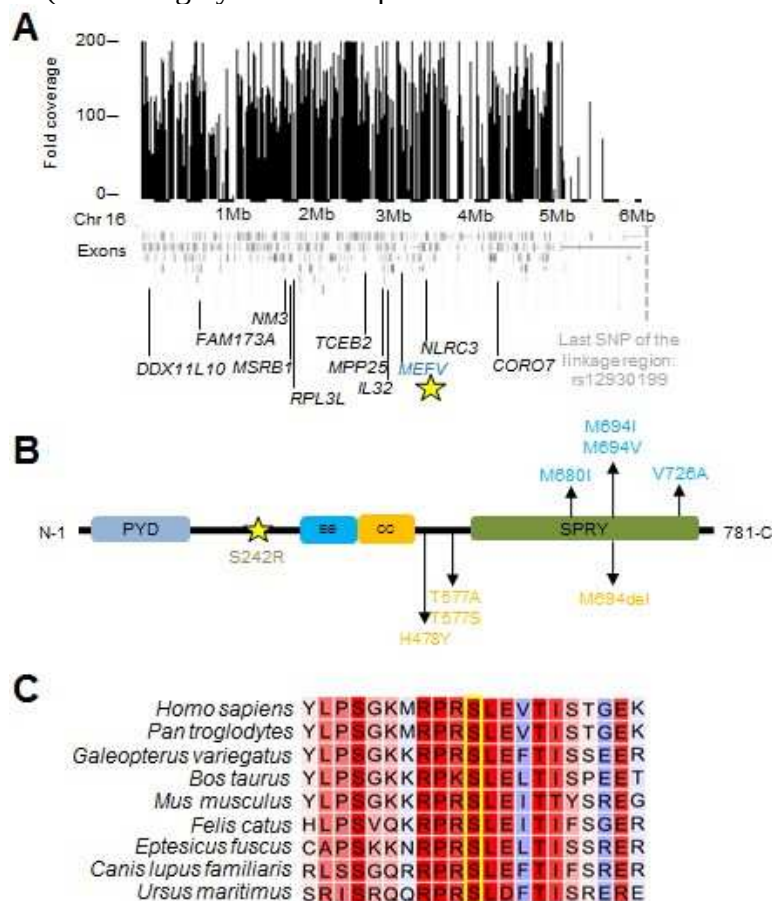


Figure S4. Inheritance of S242R mutations in additional pedigrees. (a) Known pedigree and clinical condition of a French family carrying the S242R mutation. Parental testing was not available to determine whether the mutation was inherited or de novo. **(b)** Known

pedigree and clinical condition of a Lebanese family carrying the S242R mutation. Parental testing revealed that this was a compound heterozygous allele. Gray indicates clinical testing was not possible. The mother self-reported as healthy. **(c)** Known pedigree and clinical condition of a British family carrying the S242R mutation. * transient skin rashes/nodules.



- 1. Neutrophilic dermatosis
- 2. Recurrent fever
- 3. Acute-phase reactants
- 4. Arthralgia
- 5. Myalgia
- 6. Cardiomyopathy
- 7. Anaemia
- 8. Pyogenic arthritis
- 9. Serositis

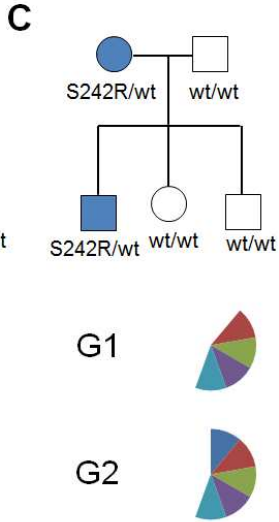
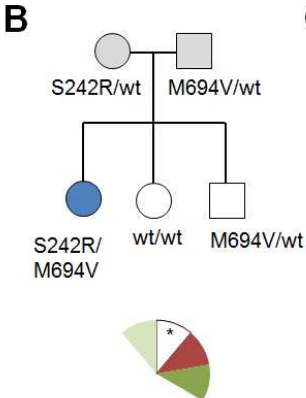
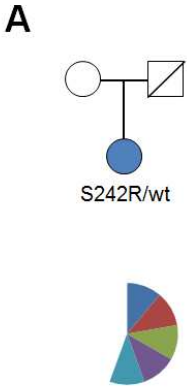


Figure S5. Fluorescent microscopy of Caspase-1 recruitment to the inflammasome.

Confocal microscopy showing a pyrin-driven increase in recruitment of GFP-Caspase-1 to cytoplasmic specks of ASC when co-transfected into HEK293T cells with wildtype or mutated pyrin (S242R). Representative of at least 3 biologically-independent experiments.

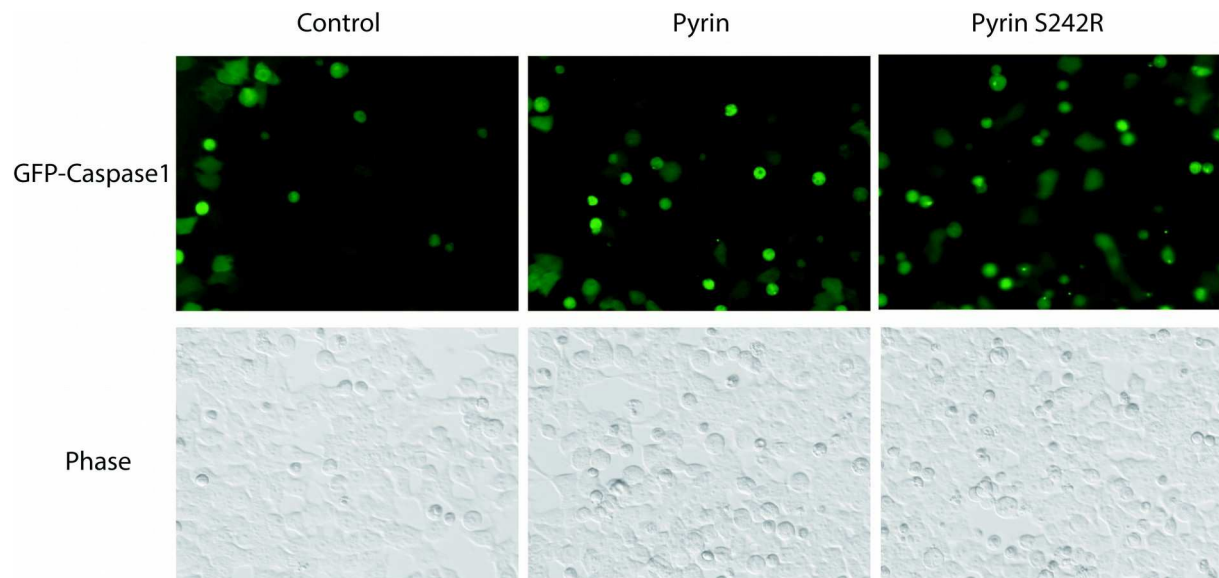
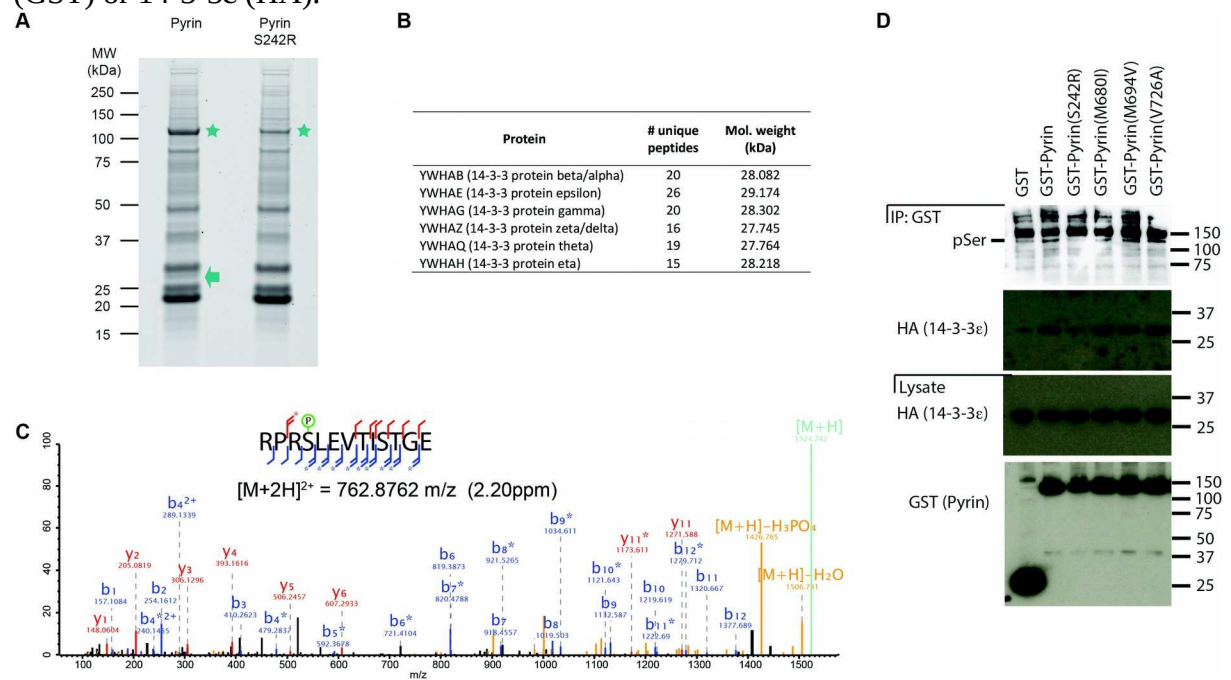


Figure S6. Proteomic analysis of pyrin interactions and phosphorylation. (a) GST-tagged pyrin with or without the S242R variant was overexpressed in HEK293T cells, then immunoprecipitated using glutathione sepharose 4B, with eluates run on a SDS-PAGE gel and stained with Sypro Ruby followed by Coomassie G-250. Stars indicate the bands corresponding to pyrin or pyrin S242R, while the band bound specifically to pyrin, indicated by an arrow, was excised for proteomic analysis. (b) Summary of the proteomic analysis for the band marked by an arrow on the SDS-PAGE gel in panel (a). (c) MS/MS spectrum identifying pyrin phosphorylation site at S242. Stars indicate neutral loss fragmentation ions, clearly demonstrating phosphate localisation at serine 242. Representative of at least 3 biologically-independent experiments. (d) GST, or GST-Pyrin variants were expressed in HEK293T cells, together with HA-14-3-3 α . Lysates or eluates from GST immunoprecipitation (IP) were subjected to western blotting for pSer (14-3-3 motif), pyrin (GST) or 14-3-3 ϵ (HA).



References

1. Antanaviciute A, Daly C, Crinnion LA, et al. GeneTIER: prioritization of candidate disease genes using tissue-specific gene expression profiles. *Bioinformatics* 2015;31:2728-35.
2. Li H, Durbin R. Fast and accurate long-read alignment with Burrows-Wheeler transform. *Bioinformatics* 2010;26:589-95.
3. McKenna A, Hanna M, Banks E, et al. The Genome Analysis Toolkit: a MapReduce framework for analyzing next-generation DNA sequencing data. *Genome research* 2010;20:1297-303.
4. Van der Auwera GA, Carneiro MO, Hartl C, et al. From FastQ data to high confidence variant calls: the Genome Analysis Toolkit best practices pipeline. *Current protocols in bioinformatics / editorial board, Andreas D Baxeavanis [et al]* 2013;11:11 0 1- 0 33.
5. Wang K, Li M, Hakonarson H. ANNOVAR: functional annotation of genetic variants from high-throughput sequencing data. *Nucleic acids research* 2010;38:e164.
6. Chae JJ, Komarow HD, Cheng J, et al. Targeted disruption of pyrin, the FMF protein, causes heightened sensitivity to endotoxin and a defect in macrophage apoptosis. *Mol Cell* 2003;11:591-604.
7. Waite AL, Schaner P, Hu C, et al. Pyrin and ASC co-localize to cellular sites that are rich in polymerizing actin. *Exp Biol Med (Maywood)* 2009;234:40-52.
8. Chae JJ, Wood G, Richard K, et al. The familial Mediterranean fever protein, pyrin, is cleaved by caspase-1 and activates NF-kappaB through its N-terminal fragment. *Blood* 2008;112:1794-803.
9. Baker PJ, Boucher D, Bierschenk D, et al. NLRP3 inflammasome activation downstream of cytoplasmic LPS recognition by both caspase-4 and caspase-5. *Eur J Immunol* 2015.
10. Huesgen PF, Lange PF, Rogers LD, et al. LysargiNase mirrors trypsin for protein C-terminal and methylation-site identification. *Nat Methods* 2015;12:55-8.
11. Hildebrand JM, Tanzer MC, Lucet IS, et al. Activation of the pseudokinase MLKL unleashes the four-helix bundle domain to induce membrane localization and necroptotic cell death. *Proc Natl Acad Sci U S A* 2014;111:15072-7.
12. Sester DP, Thygesen SJ, Sagulenko V, et al. A novel flow cytometric method to assess inflammasome formation. *J Immunol* 2015;194:455-62.